Optimal preparation of Bose and Fermi atomic gas mixtures of ^{87}Rb and ^{40}K in a crossed optical dipole trap

Peibo Ding(丁培波)[1], Biao Shan(单标)[1], Yuhang Zhao(赵宇航)[1], Yajing Yang(杨雅婧)[1], Liangchao Chen(陈良超)[1,2], Zengming Meng(孟增明)[1,2], Pengjun Wang(王鹏军)[1,2], and Lianghui Huang(黄良辉)[1,2,†]

[1] *State Key Laboratory of Quantum Optics and Quantum Optics Devices, Institute of Opto-electronics, Collaborative Innovation Center of Extreme Optics, Shanxi University, Taiyuan* 030006, *China*

[2] *Hefei National Laboratory, Hefei* 230000, *China*

(Received 3 February 2024; revised manuscript received 26 February 2024; accepted manuscript online 13 March 2024)

We report on the optimal production of the Bose and Fermi mixtures with ^{87}Rb and ^{40}K in a crossed optical dipole trap (ODT). We measure the atomic number and lifetime of the mixtures in combination of the spin state $|F=9/2, m_{\rm F}=9/2\rangle$ of ^{40}K and $|1,1\rangle$ of ^{87}Rb in the ODT, which is larger and longer compared with the combination of the spin state $|9/2,9/2\rangle$ of ^{40}K and $|2,2\rangle$ of ^{87}Rb in the ODT. We observe the atomic numbers of ^{87}Rb and ^{40}K shown in each stage of the sympathetic cooling process while gradually reducing the depth of the optical trap. By optimizing the relative loading time of atomic mixtures in the MOT, we obtain the large atomic number of ^{40}K ($\sim 6\times10^6$) or the mixtures of atoms with an equal number ($\sim 1.6\times10^6$) at the end of evaporative cooling in the ODT. We experimentally investigate the evaporative cooling in an enlarged volume of the ODT via adding a third laser beam to the crossed ODT and found that more atoms (8×10^6) and higher degeneracy ($T/T_{\rm F}=0.25$) of Fermi gases are obtained. The ultracold atomic gas mixtures pave the way to explore phenomena such as few-body collisions and the Bose–Fermi Hubbard model, as well as for creating ground-state molecules of ^{87}Rb^{40}K.

Keywords: optical dipole trap, Bose and Fermi gas mixtures, atomic lifetime

PACS: 67.85.Pq, 37.10.Jk, 03.75.Ss, 34.50.Cx **DOI:** 10.1088/1674-1056/ad334d

Ultracold atomic gas mixtures provide an exciting platform for exploring complex interesting physics, such as the observation of heteronuclear molecules,[1–3] superfluid mixtures,[4,5] Bose and Fermi polarons,[6–8] quantum droplets,[9–12] and Efimov trimers.[13,14] Two-species mixtures present special interest because of their special character with large mass imbalance and species-specific optical manipulation. These atomic mixtures can be created with the same species in different spin states[15,16] or isotopes,[17,18] two different species,[19–26] or three different species.[27,28] In addition, bosonic atoms can be used to achieve degenerate fermionic atoms through sympathetically evaporative cooling, shch as ^{7}Li–^{6}Li,[29] ^{87}Rb–^{40}K,[30] ^{23}Na–^{6}Li,[31] ^{84}Sr–^{87}Sr,[32] ^{23}Na–^{40}K,[33] ^{41}K–^{6}Li,[34] ^{133}Cs–^{6}Li,[35] ^{174}Yb–^{6}Li,[36] and ^{6}Li–^{84}Sr.[37]

The alkali-metal binary atomic Bose–Fermi mixtures with ^{87}Rb and ^{40}K exhibit intriguing properties, which have rich Feshbach resonances, and have attracted enormous attention,[38,39] such as the Bose–Fermi Hubbard model,[40] few-body and mean-field many-body,[41] realization of mixed bright solitons,[42] and creation of polar molecules.[43] However, many problems still need to be overcome to achieve the degeneracy of Bose–Fermi gas mixtures in experiments, such as increasing the number and lifetime of the atomic mixtures via reducing the light-assisted hetero-nuclear collision losses,[44] avoiding the space competition induced by the overlap high densities of the two atomic clouds during the stage for capturing atoms in three-dimensional magnetic-optical trap (3D MOT), and finding the right spin state to form atomic mixtures and to achieve better sympathetically evaporative cooling effect in the optical dipole trap (ODT).

In this work, we report different technologies employed aiming to optimize the production of the Bose and Fermi mixtures with ^{87}Rb and ^{40}K in the ODT. We measure the atomic number and lifetime of the mixtures at the combination of the spin state $|F=9/2, m_{\rm F}=9/2\rangle$ of ^{40}K and $|1,1\rangle$ of ^{87}Rb in the ODT, which is larger and longer compared with the combination of the spin state $|9/2,9/2\rangle$ of ^{40}K and $|2,2\rangle$ of ^{87}Rb. We observe the atomic numbers of ^{87}Rb and ^{40}K in each stage of the sympathetic cooling process while gradually reducing the depth of the optical trap. As we fix the total loading time and sweep the loading time of the ^{87}Rb, we obtain a function via changing the loading time of ^{87}Rb and ^{40}K atoms in ODT. The ratio of mixtures for ^{87}Rb and ^{40}K can be adjusted easily by controlling the different MOT loading times of the two species. Additionally, we conduct experimental research on evaporative cooling in a larger volume of ODT by adding a third laser beam to the crossed dipole trap. At the end of evaporative cooling in the ODT, a higher atomic number and higher degeneracy of Fermi gases are achieved.

The construction of the apparatus is shown in Fig. 1(a), comprising 2D MOT and 3D MOT configurations for ^{87}Rb and

†Corresponding author. E-mail: huanglh06@sxu.edu.cn

^{40}K, as previously described in Refs. [44–46]. The 2D MOT chamber is composed of four rectangular light windows with a size of 150 mm × 40 mm and the 3D MOT science cell is a glass cell with a size of 100 mm × 40 mm × 40 mm. Through the operation of two ion pumps (40 L/s and 150 L/s), the vapor pressure of the 2D chamber and the 3D science cell are maintained around 10^{-7} Pa and 10^{-9} Pa, respectively. Initially, ^{87}Rb and ^{40}K are loaded from the background vapor in the 2D MOT produced by dispensers. To avoid spatial competition induced by the overlap of high densities in both clouds[47] during the loading phase in the 3D MOT, we adopt a staggered loading approach. Initially, we capture the ^{40}K atomic sample in a dual dark magnetic-optical trap for approximately 60 s, followed by the concurrent loading of the ^{87}Rb atomic sample and the ^{40}K atomic sample in the last 10 s, and the timing sequence is shown in Fig. 1(b). Then, the optical molasses step follows the compressed MOT (CMOT). Here, the ^{87}Rb atoms are cooled by the molasses of the D2 line while the ^{40}K atoms are applied by the gray molasses of the D1 line[25,48] shown in Fig. 1(b). Afterwards, the atomic mixtures are prepared at $|2,2\rangle$ for ^{87}Rb and $|9/2,9/2\rangle$ for ^{40}K using an optical pumping stage, which are the weak-field seeking states. Then, the atomic mixtures are further cooled via radio-frequency evaporative cooling in a combined trap consisting of an optical plug and a quadrupole magnetic trap.[49] Typically, 2.6×10^7 of ^{40}K$|9/2,9/2\rangle$ at 18.6 μK and 4.2×10^7 of ^{87}Rb$|2,2\rangle$ at 15.4 μK are obtained at the end of the evaporative cooling in the combined trap.

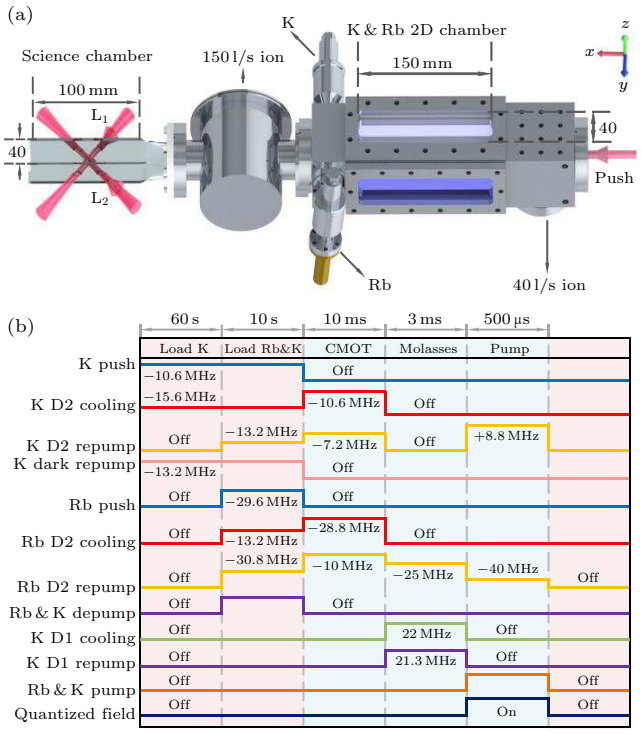

Fig. 1. Schematic of experimental scheme and timing diagram at MOT stage. (a) Front view of the compact vacuum system for the preparation for Bose–Fermi mixtures, including two parts for precooling of ^{87}Rb and ^{40}K in 2D MOT chamber, and MOT, CMOT, molasses in 3D MOT chamber. (b) Experimental sequence for the loading and cooling processes in MOT.

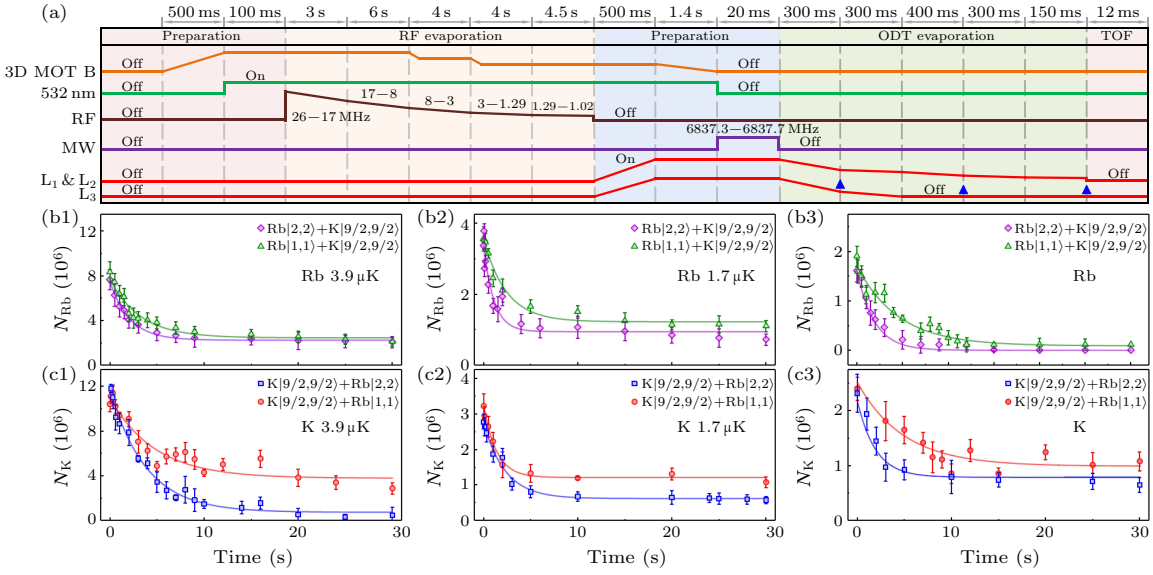

Fig. 2. Experimental sequence and lifetimes of atomic mixtures ^{87}Rb and ^{40}K at the end of first, third and last steps of the evaporative cooling in ODT. (a) Experimental sequence for the loading processes in ODT. The blue triangles indicate the position for each step in the ODT. (b1)–(b3) The lifetimes of ^{87}Rb in combination of various mixture states of ^{87}Rb$|2,2\rangle$+^{40}K$|9/2,9/2\rangle$ (purple diamond) and ^{87}Rb$|1,1\rangle$+^{40}K$|9/2,9/2\rangle$ (green triangle) at the end of 1st, 3rd, and 5th steps in ODT, respectively. The solid lines show the numerical fits to the experimental data, which give the atomic lifetime of ^{87}Rb$|2,2\rangle$ and $|1,1\rangle$ in the combination with ^{40}K$|9/2,9/2\rangle$ at the closed value 2.6 s & 2.8 s (b1), 2.5 s & 3 s (b2), and 2 s & 4.4 s (b3). (c1)–(c3) The atomic lifetime of the ^{40}K with ^{87}Rb atom in $|2,2\rangle$ state (blue square) and $|1,1\rangle$ state (red dot) at the end of 1st, 3rd, and 5th steps in ODT, respectively. The solid lines show the numerical fits to the experimental data, which give the atomic lifetime of ^{40}K$|9/2,9/2\rangle$ in the combination with $|2,2\rangle$ and $|1,1\rangle$ of ^{87}Rb at the values of 3.7 s & 4.8 s (c1), 3.7 s & 4.7 s (c2), and 3.7 s & 5 s (c3). The error bars indicate the standard error of the mean of three experimental runs.

Firstly, the atomic mixtures are transferred into a far-detuning ODT to realize the evaporation in five steps via ramping down the depth of dipole trap. Here, the ODT is formed by two beams (L_1 3.4 W & L_2 2.3 W) at a wavelength of 1064 nm with waist radii of 50 μm and 45 μm crossing in the $(\hat{x}\pm\hat{y})$ horizontal plane, as shown in Fig. 1(a). We measure the lifetime of mixtures at the first (1st), third (3rd), and last (5th) steps of the evaporative cooling in the ODT shown in Figs. 2(b) and 2(c). After the atoms are transferred into the ODT at the desired step, a rapid spin state transfer process is performed to prepare the atomic sample $|1,1\rangle$ of ^{87}Rb via the Landau–Zener process through an MW driven transition during 20 ms at external magnetic field of 2.7 G defined as the spin quantization axis. The remaining atoms at $|2,2\rangle$ state are removed via shining a resonant laser radiation (780 nm) for 0.03 ms to avoid the ^{40}K atoms heating and losing. In our experiments, we fit the experimental data with a single exponential function and extract the lifetime of the atomic gases. The fitting equation for the lifetime reads[50]

$$N = N_0\,\mathrm{e}^{-t/\tau} + N_\mathrm{r}, \tag{1}$$

where N_0+N_r is the initial total number of atoms when $t=0$, N_r is the constant number of atoms finally remaining in the trap, and τ is the lifetime. For the spin state mixtures of ^{87}Rb$|2,2\rangle$+^{40}K$|9/2,9/2\rangle$ and ^{87}Rb$|1,1\rangle$+^{40}K$|9/2,9/2\rangle$, we find that the atomic lifetime and number of ^{87}Rb at spin state $|2,2\rangle$ and $|1,1\rangle$ are basically same during the sympathetic cooling process for ^{40}K, as shown in Fig. 2(b1). However, the lifetime of the first step evaporating in ODT is different from the mixtures of ^{40}K$|9/2,9/2\rangle$+^{87}Rb$|2,2\rangle$ and ^{40}K$|9/2,9/2\rangle$+^{87}Rb$|1,1\rangle$, respectively, as shown in Fig. 2(c1). For the spin state mixtures $|1,1\rangle$ of ^{87}Rb and $|9/2,9/2\rangle$ of ^{40}K, the lifetime can be increased to about 4.8 s. Note that we have tried the combination of the spin state $|9/2,9/2\rangle$ of ^{40}K and $|2,2\rangle$ of ^{87}Rb in the ODT, and the atomic lifetime of ^{40}K is only around 3.7 s, as shown in Fig. 2(c1). The lifetime of the mixtures at the end of third step in ODT are observed via reducing the depth of the optical trap, as shown in Figs. 2(b2) and 2(c2). We find that the lifetime of $|1,1\rangle$ is longer than the $|2,2\rangle$ for ^{87}Rb and ^{40}K, as shown in Figs. 2(b2) and 2(c2). At the end of the ODT, the difference between $|1,1\rangle$ and $|2,2\rangle$ is even more pronounced. For ^{87}Rb, the lifetime of $|2,2\rangle$ and $|1,1\rangle$ are 2 s and 4.4 s, as shown in Fig. 2(b3). For ^{40}K, the lifetime of $|2,2\rangle$ and $|1,1\rangle$ are 3.7 s and 5 s, as shown in Fig. 2(c3). It should be noted that in the ODT, the atomic collisional rate and the losses of atomic collision are substantially enhanced compared with a typical MOT due to the low atomic density. In the process of magnetic trap evaporation, there is no significant difference in the atomic collision losses of the two states of ^{87}Rb due to the relatively low atomic number density. In addition, the loss induced by the atomic collision in the ODT with the combination of ^{87}Rb$|2,2\rangle$ and ^{40}K$|9/2,9/2\rangle$ is more serious than the combination of ^{87}Rb$|1,1\rangle$ and ^{40}K$|9/2,9/2\rangle$. Compared to the spin combination of ^{87}Rb$|2,2\rangle$+^{40}K$|9/2,9/2\rangle$, the longer lifetimes of the spin combination of ^{87}Rb$|1,1\rangle$+^{40}K$|9/2,9/2\rangle$ may be induced by following reasons. Firstly, the spin combination of ^{87}Rb$|2,2\rangle$+^{40}K$|9/2,9/2\rangle$ is more likely to be lost through other loss channels because the spin combination of ^{87}Rb$|2,2\rangle$+^{40}K$|9/2,9/2\rangle$ has higher energy than ^{87}Rb$|1,1\rangle$+^{40}K$|9/2,9/2\rangle$.[51,52] Secondly, the hyperfine-changing collision for the combinations of ^{87}Rb$|1,1\rangle$+^{40}K$|9/2,9/2\rangle$ is a process of energy absorption and is forbidden.[53–55] Thirdly, the difference of heteronuclear elastic collision rates ($-235a_0$ and $-430a_0$)[56] is a reason for the longer lifetime. Finally, the longer lifetime of ^{87}Rb $|1,1\rangle$ and fast thermalization of ^{87}Rb$|1,1\rangle$+^{40}K$|9/2,9/2\rangle$ are also a reason for the spin combination of ^{87}Rb$|1,1\rangle$+^{40}K$|9/2,9/2\rangle$ maintaining longer lifetimes.

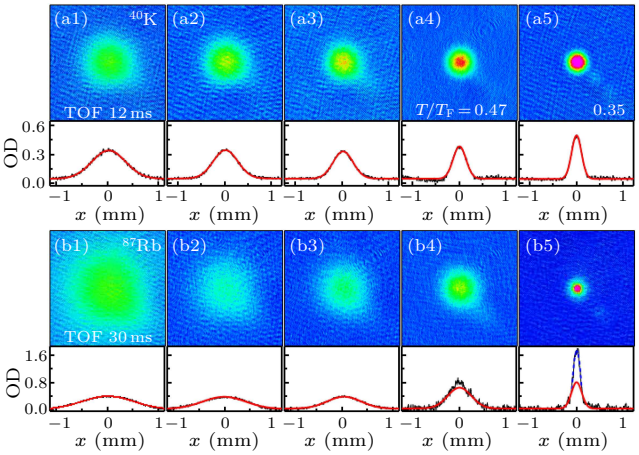

Fig. 3. Atomic time of absorption imaging (TOF) for atomic mixtures ^{87}Rb and ^{40}K at each stage when the depth of ODT is decreased adiabatically. (a1)–(a5) TOF images of ^{40}K correspond to five steps in ODT with ^{87}Rb, and the time of TOF is 12 ms. The curve at the bottom of the figure is the integral for the optical density of the ^{40}K atomic profile. The atomic numbers are 5.1×10^6, 4.2×10^6, 3.4×10^6, 2.9×10^6, 2.6×10^6, respectively. (b1)–(b5) TOF images of ^{87}Rb correspond to five steps in ODT with ^{40}K, and the time of TOF is 30 ms. The curve at the bottom of the figure is the integral for the optical density of the ^{87}Rb atomic profile. The blue dashed line represents a fit with a bimodal distribution, while the red solid line denotes a Gaussian fit to the thermal part. The atomic numbers are 4.9×10^6, 3.5×10^6, 3×10^6, 2.4×10^6, and 0.8×10^6, respectively. The image size is 2.2 mm × 2.2 mm.

Afterwards, we observe the atomic number of ^{87}Rb shown in Figs. 3(a1)–3(a5) and ^{40}K shown in Figs. 3(b1)–3(b5) at each stage in the sympathetic cooling process through gradually reducing the depth of the ODT shown in Fig. 2(a). It is shown that the atomic numbers of ^{87}Rb and ^{40}K decrease simultaneously at each stage of the evaporation in the crossed ODT, and the atoms ^{87}Rb still exist even the number of ^{40}K atoms is at its maximum, which ensures that we can obtain a standard atomic sample number by optimizing all steps in the ODT. Nearly $N=2.6\times10^6$ ultracold ^{40}K atoms

are prepared at a temperature of 0.35 T_F during the process of sympathetic cooling with ^{87}Rb, where $T_F = \hbar\bar{\omega}$ is the Fermi temperature,[57] $\bar{\omega} = (\omega_x\omega_y\omega_z)^{1/3} \simeq 2\pi \times 80$ Hz is the geometric mean of the optical trap in our experiment, N is the particle number of ^{40}K atoms, and k_B is Boltzmann's constant. As we decrease the intensity of the ODT step by step shown in Fig. 2(a), the degeneracy of the ^{40}K atom eventually decreases to 0.35, and the atomic optical density (OD) increases from its integration shown in Figs. 3(a1)–3(a5). Meanwhile, Bose–Einstein condensation (BEC) of ^{87}Rb of 0.8×10^6 atoms can also be observed after the last step of evaporation shown in Fig. 3(b5).

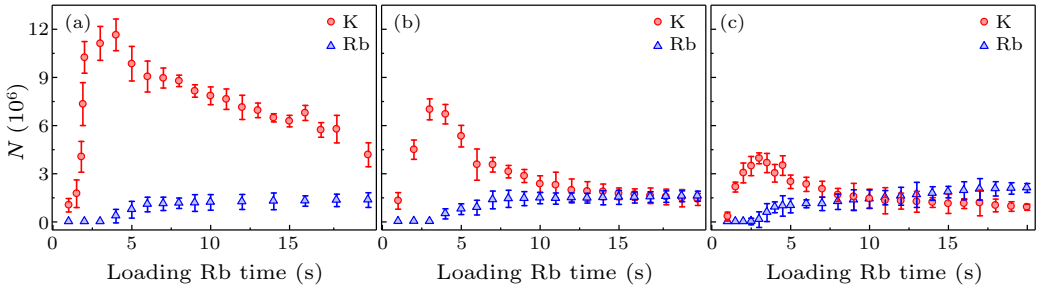

Fig. 4. The particle numbers of atomic mixtures for ^{40}K (red circle) and ^{87}Rb (blue triangle) in the ODT at the last evaporation as a function of the loading time for ^{87}Rb in MOT. Initially, the total loading times are fixed at 70 s (a), 50 s (b), and 35 s (c), while ^{87}Rb is loaded with ^{40}K at the same time in subsequent cycles. The error bars indicate the standard error of the mean of three experimental runs.

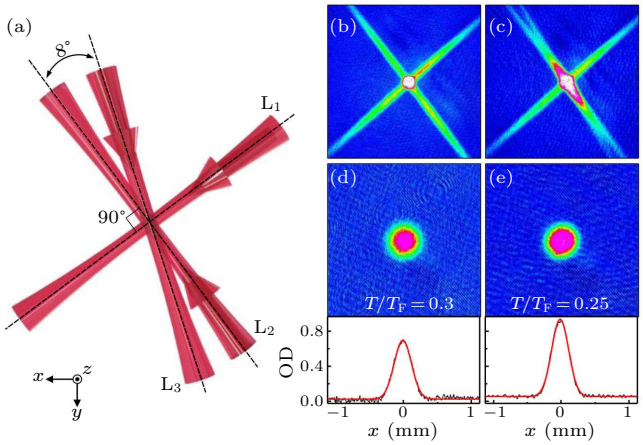

Fig. 5. (a) The enlarged ODT consisting of three far-off resonant 1064 nm crossed laser beams (L_1 & L_2 & L_3) in the $(\hat{x} \pm \hat{y})$ horizontal plane. L_1 and L_2 are perpendicular to each other while there is only a small intersection angle ($\sim 8°$) between L_2 and L_3. Atomic absorption imaging of ^{87}Rb by two far red detuned laser beams with L_1 & L_2 (b) and L_1 & L_2 & L_3 (c). The magnetic trap is directly switched off after loading ^{87}Rb into the ODT. Subsequently, the ODT holds on with maximum power during the first 38 ms while it is closed during the last 2 ms for free flight process. The size of images in (b) and (c) is 3.2 mm × 3.2 mm. TOF image of ^{40}K at the end of the evaporation cooling in ODT with L_1 & L_2 (d) and L_1 & L_2 & L_3 (e), and the time of TOF is 12 ms. The size of images in (d) and (e) is 2.2 mm × 2.2 mm.

In addition, we observe the atomic mixture of ^{87}Rb and ^{40}K atoms at the end of evaporation in the ODT as a function via changing the loading time of ^{87}Rb and ^{40}K atoms in MOT, as shown in Fig. 4. Here, the total loading time of ^{40}K in MOT is fixed at 70 s, 50 s, and 35 s. Figure 4(a) shows the maximum number (1.1×10^7) of ^{40}K atoms prepared when the loading time of ^{87}Rb is around 4 s, and the total loading time is fixed at 70 s, accompanied by a small number of ^{87}Rb atoms in ODT. Figure 4(b) shows the normal atomic number (6×10^6) of ^{40}K atoms prepared when the loading time for ^{87}Rb is around 4.5 s and the total loading time is fixed at 50 s. Figure 4(c) shows a smaller atomic number (4×10^6) of ^{40}K atoms prepared when the loading time for ^{87}Rb is around 5 s and the total loading time is fixed at 35 s. From Figs. 4(a)–4(c), we find that the number of ^{87}Rb atoms in the ODT only increases slightly as the loading time of ^{40}K atoms decreases, basically remaining at $\sim 1.8 \times 10^6$. Moreover, the atomic numbers of ^{87}Rb and ^{40}K are equal when the loading time for ^{87}Rb is 10 s and the total loading time is 35 s, which can provide a good reference for us to create the equal mixtures or different proportions of ^{87}Rb and ^{40}K. It should be noted that we can prepare a pure Bose–Einstein condensate (BEC) of ^{87}Rb atoms with 2.6×10^6 using the same way if we only take 10 s to load ^{87}Rb atoms into MOT without loading of ^{40}K, and the lifetimes of the pure BEC of $|2,2\rangle$ and $|1,1\rangle$ are around 3.2 s and 7 s.

Finally, we also add the third far-detuning laser beam to the ODT with a small intersection angle ($\sim 8°$) to increase the atom loading efficiency via expanding the volume[24] of the dipole trap shown in Fig. 5(a). Figure 5(b) shows the image of atomic absorption of ^{87}Rb with two far-red detuned laser beams (L_1 & L_2) at the angle of around 90°. Figure 5(c) shows the image of atomic absorption of ^{87}Rb with three far-red detuning laser beams (L_1 & L_2 & L_3) at the small angle around 8° between L_2 and L_3. First, the mixtures are loaded into the larger volume of ODT through increasing the depth of the ODT to full intensity of the three far-detuning lasers (L_1 3.4 W&L_2 2.3 W & L_3 1.8 W) during 500 ms. The powers of L_1 and L_2 beams are the same as that of the two-beam evaporative cooling scheme. Then, the power of the three laser beams is reduced to realize the forced evaporation of the mixtures in the ODT during the second step. Afterwards, the intensity of the third laser beam (L_3) with a waist radius of 45 μm is ramped down to zero firstly to increase the atomic collision rate via decreasing the volume of ODT in the third step. At the end of evaporative cooling in the ODT, the atomic number of ^{40}K in the trap (L_1 & L_2 & L_3) can reach up to 8×10^6 with higher atomic density. This represents an increase of 30%

compared to the atomic number in the ODT composed of two far-detuned lasers (L_1 & L_2), as shown in Figs. 5(e) and 5(d). Meanwhile, the degeneracy of Fermi gases is reduced from $T/T_F = 0.30$ in the ODT with two laser beams to 0.25 in the ODT with three laser beams. At the beginning of the loading process, the three-beam configuration can increase the loading volume and decrease the trap frequency compared with the two-beam case, which helps to load enough thermal atoms from the magnetic trap to form a larger thermal atomic cloud. During the evaporative cooling process, the intensity of the third laser beam (L_3) is ramped down to zero in the third step to increase the atomic collision rate via decreasing the volume of ODT.

In conclusion, we optimize the production of the Bose and Fermi mixtures with ^{87}Rb and ^{40}K in the ODT. We measure the atomic number and lifetime of the mixtures at the combination with the spin state $^{40}\mathrm{K}|9/2,9/2\rangle+^{87}\mathrm{Rb}|1,1\rangle$ in the ODT, which is larger and longer than the combination with the spin state $^{40}\mathrm{K}|9/2,9/2\rangle+^{87}\mathrm{Rb}|2,2\rangle$ in 1st, 3rd, and 5th steps of ODT. During the five steps of evaporation cooling in ODT, we measure the atomic numbers of ^{87}Rb and ^{40}K in each stage via reducing the depth of the ODT gradually. We obtain the relationship between atomic number of mixtures and loading time of ^{87}Rb while the total loading time is fixed, which allows us to precisely control the ratio between ^{87}Rb and ^{40}K. We also experimentally investigate the evaporative cooling in a larger volume of ODT via adding a third laser beam with a small angle to the crossed ODT, and achieve a higher atomic number and higher degeneracy of Fermi gases. Due to the different physical properties of ^{87}Rb and ^{40}K, their ultracold Bose–Fermi mixtures are an excellent candidate for a stable heteronuclear system allowing the study of several quantum phenomena that have not yet been explored.

Acknowledgments

This research was supported by the Innovation Program for Quantum Science and Technology (Grant No. 2021ZD0302003), the National Natural Science Foundation of China (Grant Nos. 12034011, U23A6004, 12374245, 12322409, 92065108, 11974224, and 12022406), the National Key Research and Development Program of China (Grant Nos. 2022YFA1404101 and 2021YFA1401700), and the Fund for Shanxi 1331 Project Key Subjects Construction.

References

[1] Ni K K, Ospelkaus S, Jin D S and Ye J 2008 *Science* **322** 231
[2] Voigt A C, Taglieber M and Dieckmann K 2009 *Phys. Rev. Lett.* **102** 020405
[3] Takekoshi T, Le Sueur C R and Grimm R 2014 *Phys. Rev. Lett.* **113** 205301
[4] Ferrier-Barbut I, Delehaye M and Salomon C 2014 *Science* **345** 1035
[5] Roy R, Green A, Bowler R and Gupta S 2017 *Phys. Rev. Lett.* **118** 055301
[6] Cetina M, Jag M, Lous R S, Walraven J T M, Grimm R, Christensen R S and Bruun G M 2015 *Phys. Rev. Lett.* **115** 135302
[7] Hu M G, Van de Graaff M J, Kedar D, Corson J P, Cornell E A and Jin D S 2016 *Phys. Rev. Lett.***117** 055301
[8] Scazza F, Valtolina G, Massignan P, Recati A, Amico A, Burchianti A, Fort C, Inguscio M, Zaccanti M and Roati G 2017 *Phys. Rev. Lett.* **118** 083602
[9] Petrov D S 2015 *Phys. Rev. Lett.* **115** 155302
[10] Cabrera C R, Tanzi L, Sanz J, Naylor B, Thomas P, Cheiney P and Tarruell L 2018 *Science* **359** 301
[11] Semeghini G, Ferioli G, Masi L, Mazzinghi C, Wolswijk L, Minardi F, Modugno M, Modugno G, Inguscio M and Fattori M 2018 *Phys. Rev. Lett.* **120** 235301
[12] Cheiney P, Cabrera C R, Sanz J, Naylor B, Tanzi L and Tarruell L 2018 *Phys. Rev. Lett.* **120** 135301
[13] Naidon P and Endo S 2017 *Rep. Prog. Phys.* **80** 056001
[14] Greene C H, Giannakeas P and Pérez-Ríos J 2017 *Rev. Mod. Phys.* **89** 035006
[15] Myatt C J, Burt E A, Ghrist R W, Cornell E A and Wieman C E 1997 *Phys. Rev. Lett.* **78** 586
[16] Maddaloni P, Modugno M, Fort C, Minardi F and Inguscio M 2000 *Phys. Rev. Lett.* **85** 2413
[17] Schreck F, Khaykovich L, Corwin K L, Ferrari G, Bourdel T, Cubizolles J and Salomon C 2001 *Phys. Rev. Lett.* **87** 080403
[18] Fukuhara T, Sugawa S, Takasu Y and Takahashi Y 2009 *Phys. Rev. A* **79** 021601
[19] Ospelkaus C, Ospelkaus S, Sengstock K and Bongs K 2006 *Phys. Rev. Lett.* **96** 020401
[20] Best T, Will S, Schneider U, Hackermüller L, van Oosten D, Bloch I and Lühmann D S 2009 *Phys. Rev. Lett.* **102** 030408
[21] McCarron D J, Cho H W, Jenkin D L, Koppinger M P and Cornish S L 2011 *Phys. Rev. A* **84** 011603
[22] Park J W, Wu C H, Santiago I, Tiecke T G, Will S, Ahmadi P and Zwierlein M W 2012 *Phys. Rev. A* **85** 051602
[23] Wang F, Li X, Xiong D and Wang D 2016 *J. Phys. B: At. Mol. Opt. Phys.* **49** 015302
[24] Warner C, Lam A Z, Bigagli N, Liu H C, Stevenson I and Will S 2021 *Phys. Rev. A* **104** 033302
[25] Li Z, Gu Z, Shi Z, Wang P and Zhang J 2023 *Chin. Phys. B* **32** 023701
[26] Chen Y D, Li W X, Sun Y T, Chen Q C, Chang P Y and Tung S 2023 *Phys. Rev. A* **108** 033301
[27] Taglieber M, Voigt A C, Aoki T, Hänsch T W and Dieckmann K 2008 *Phys. Rev. Lett.* **100** 010401
[28] Salasnich L and Toigo F 2007 *Phys. Rev. A* **75** 013623
[29] Truscott A G, Strecker K E, McAlexander W I, Partridge G B and Hulet R G 2001 *Science* **291** 2570
[30] Roati G, Riboli F, Modugno G and Inguscio M 2002 *Phys. Rev. Lett.* **89** 150403
[31] Hadzibabic Z, Stan C A, Dieckmann K, Gupta S, Zwierlein M W, Gorlitz A and Ketterle W 2002 *Phys. Rev. Lett.* **88** 160401
[32] Tey M K, Stellmer S, Grimm R and Schreck F 2010 *Phys. Rev. A* **82** 011608
[33] Wu C H, Santiago I, Park J W, Ahmadi P and Zwierlein M W 2011 *Phys. Rev. A* **84** 011601
[34] Yao X C, Chen H Z, Wu Y P, Liu X P, Wang X Q, Jiang X, Deng Y, Chen Y A and Pan J W 2016 *Phys. Rev. Lett.* **117** 145301
[35] DeSalvo B J, Patel K, Johansen J and Chin C 2017 *Phys. Rev. Lett.* **119** 233401
[36] Schafer F, Konishi H, Bouscal A, Yagami T and Takahashi Y 2017 *Phys. Rev. A* **96** 032711
[37] Ye Z X, Xie L Y, Guo Z, Ma X B, Wang G R, You L and Tey M K 2020 *Phys. Rev. A* **102** 033307
[38] Wang P J, Fu Z K, Chai S J and Zhang J 2011 *Chin. Phys. B* **20** 103401
[39] Huang L, Wang P, Fu Z and Zhang J 2014 *Chin. Phys. B* **23** 013402
[40] Schönmeier-Kromer J and Pollet L 2023 *Phys. Rev. B* **107** 054502
[41] Parajuli B, Pecak D and Chien C C 2023 *Phys. Rev. A* **107** 023308

[42] Inouye S, Goldwin J, Olsen M L, Ticknor C, Bohn J L and Jin D S 2004 *Phys. Rev. Lett.* **93** 183201

[43] De Marco L, Valtolina G, Matsuda K, Tobias W G, Covey J P and Ye J 2019 *Science* **363** 853

[44] Miao J, Bian G, Shan B, Chen L, Meng Z, Wang P, Huang L and Zhang J 2022 *Chin. Phys. B* **31** 080306

[45] Chai S, Wang P J, Fu Z, Huang L and Zhang J 2012 *Acta Sin. Quantum Opt.* **18** 171 (in Chinese)

[46] Huang L, Meng Z, Wang P, Peng P, Zhang S L, Chen L, Li D, Zhou Q and Zhang J 2016 *Nat. Phys.* **12** 540

[47] Goldwin J, Papp S B, DeMarco B and Jin D S 2002 *Phys. Rev. A* **65** 021402

[48] Rio Fernandes D, Sievers F, Kretzschmar N, Wu S, Salomon C and Chevy F 2012 *Europhys. Lett.* **100** 63001

[49] Davis K B, Mewes M O, Andrews M R, van Druten N J, Durfee D S, Kurn D M and Ketterle W 1995 *Phys. Rev. Lett.* **75** 3969

[50] Park J W, Will S A and Zwierlein M W 2015 *Phys. Rev. Lett.* **114** 205302

[51] Hensler S, Werner J, Griesmaier A, Giovanazzi S and Rzażewski K 2003 *Appl. Phys. B* **77** 765

[52] Krauser J S, Heinze J, Gotze S, Langbecker M, Fläschner N, Cook L, Hanna T M, Tiesinga E, Sengstock K and Becker C 2017 *Phys. Rev. A* **95** 042701

[53] Mi C D, Nawaz K S, Wang P J, Chen L C, Meng Z M, Huang L and Zhang J 2021 *Chin. Phys. B* **30** 063401

[54] Nie L, Mi C D, Zhang Y, Chen L C and Zhang J 2022 *Acta Sin. Quantum Opt.* **28** 215 (in Chinese)

[55] Wang X Q, Wang Y X, Liu X P, Pan J W, Yao X C, Chen Y A and Pan J W 2020 *Phys. Rev. A* **101** 041601

[56] Simoni A, Ferlaino F, Roati G, Modugno G and Inguscio M 2003 *Phys. Rev. Lett.* **90** 163202

[57] Bian G, Shan B, Huang L and Zhang J 2003 *Chin. Opt. Lett.* **21** 100201